Journal of King Saud University - Science 36 (2024) 103547

Contents lists available at ScienceDirect

Journal of King Saud University - Science

journal homepage: www.sciencedirect.com

Full length article

An inertial conjugate gradient projection method for large-scale nonlinear equations and its application in the image restoration problems

Gonglin Yuan [a], Chunzhao Liang [a,*], Yong Li [b]

[a] School of Mathematics and Information Science & Center of Applied Mathematics for Guangxi (Guangxi University), Nanning, Guangxi, 530004, PR China
[b] Department of Mathematics, Baise University, Baise 533000, Guangxi, China

ARTICLE INFO

Keywords:
Monotone equations
Inertial extrapolation technique
Three-term PRP method
Global convergence

ABSTRACT

Based on the acceleration effect of the inertial extrapolation technique on the convergence of iterative sequences, the number of algorithms incorporating this technique has gradually increased in recent years. Currently, there is a relative paucity of studies focusing on the Polak-Ribière-Polyak (PRP) conjugate gradient algorithm that integrate the inertial extrapolation technique. In this article, we introduce an inertial three-term PRP conjugate gradient projection method by incorporating an inertial extrapolation step into the three-term PRP algorithm, where the search direction exhibits sufficient descent and trust region characteristics. The search rule employs a derivative-free technique. Under suitable hypotheses, the proposed algorithm demonstrates global convergence. Numerical results indicate the superiority and competitiveness of this innovative method. Furthermore, its effectiveness in addressing image restoration problems underscores the practicality of this algorithm.

1. Introduction

Many practical problems can be approximated using the following model:

$$\Omega(x) = 0, \tag{1.1}$$

where $\Omega : R^n \to R^n$ is a mapping with monotone continuous characteristics. The system (1.1) is a well-known model of nonlinear monotone equations. The monotonicity of the mapping Ω indicates that it satisfies $\big(\Omega(x) - \Omega(y)\big)^T (x - y) \geq 0, \quad \forall x, y \in R^n.$

As a category of optimization problems, system (1.1) is not only extensively employed in the field of mathematics but also closely linked to real-world production and life. For instance, notable nonlinear fracture problems (Gregory et al., 1985) mathematics, chemical equilibrium issues (Meintjes and Morgan, 1987) that significantly influence industrial production, and image recovery challenges in the domain of compressed sensing (Xiao et al., 2011) can all be transformed into system (1.1) for resolution.

In recent decades, Various numerical iterative methods have been proposed to solve system (1.1). Notably, the incorporation of projection techniques (Solodov and Svaiter, 1999) has significantly enhanced the running speed of many iterative algorithms. These projection algorithms are categorized into two types: derivative-based algorithms and derivative-free algorithms. The former includes Newton-type method (Solodov and Svaiter, 1999; Zhou and Toh, 2005), quasi-Newton method (Zhou and Li, 2007, 2008; Chen et al., 2014), semi-smooth Newton method (Xiao et al., 2018) and trust region algorithm (Qi et al., 2004; Ulbrich, 2001). While these algorithms offer a rapid convergence rate as a primary advantage, the necessity of computing and storing the Jacobian or its approximate matrices poses challenges in solving large-scale equations, potentially reducing their efficiency and increasing computational time in practical applications. Consequently, the second category of methods, which does not require the computation and storage of Jacobian or its approximate matrices, has been developed to address these issues and ultimately enhance computational speed. The conjugate gradient (CG) method is a prominent example. Following the introduction of projection technology, Liu and Feng (2019) proposed a derivative-free projection method (DFPM) combined with the (PDY) method for convex constraint problems, demonstrating its Q-linear convergence. Subsequently, Sabi'U et al. (2020) introduced a new hybrid method that integrates the Fréchet-Robinson (FR) method and the PRP method with the projection strategy for monotone nonlinear equations, achieving a convergence rate significantly faster than that of the three-term PRP algorithm. For

* Corresponding author.
E-mail addresses: glyuan@gxu.edu.cn (G. Yuan), lujunwei2024@126.com (C. Liang), liyong9922@sohu.com (Y. Li).

https://doi.org/10.1016/j.jksus.2024.103547
Received 10 June 2024; Received in revised form 13 November 2024; Accepted 17 November 2024
Available online 1 December 2024

the same problems, Abubakar et al. (2021) modified a memoryless symmetric rank-one (SR1) update to develop two new algorithms, asserting their robustness. Afterward, numerous derivative-free projection methods has been proposed subsequently (Sabi'u et al., 2020; Koorapetse et al., 2021; Yin et al., 2021b,a; Sabi'u et al., 2024).

Many scholars aspire to enhance the convergence speed of iterative algorithms, leading to numerous attempts in this area (Chen et al., 2013; Iiduka, 2012; Jolaoso et al., 2021; Abubakar et al., 2020a,b, 2019). Recently, an inertial extrapolation technique has been proposed that can effectively accelerate the iteration process (Alvarez, 2004; Alvarez and Attouch, 2001). This technique, derived from the "heavy ball" method (Polyak, 1964), plays a importance role in improving the overall convergence rate of the algorithm.

Based on the acceleration effect of the inertial extrapolation technique on the convergence of iterative sequences, the number of algorithms incorporating this technique has gradually increased. For instance, this technique has been utilized to enhance various existing splitting methods (Chen et al., 2015; Pock and Sabach, 2016) and projection methods. A series of inertial DFPMs (Jian et al., 2022) have been proposed to address pseudo-monotone equations. In the field of compressed sensing, Ma et al. (2023) improved an inertial three-term CG projection method. Additionally, for convex constrained problems, an inertial Dai-Liao CG method has been proposed, which avoids the direction of maximum magnification (Sabi'U and Sirisubtawee, 2024).

Motivated by the derivative-free search strategy and the three-term PRP CG method in Yuan and Zhang (2015), we have incorporated an extrapolation strategy (Ibrahim et al., 2021) to develop the inertial three-term PRP CG projection algorithm, referred to as the ITTPRP algorithm. Under suitable conditions, we demonstrate that this new algorithm exhibits global convergence. Ultimately, a series of numerical results validate the superiority of the proposed algorithm.

The chapters of this article are organized as follows: In Section 2, we will present the ITTPRP algorithm. Section 3 provides a proof of convergence for the ITTPRP method. In Section 4, we will display results that validate the effectiveness of the ITTPRP method. Finally, Section 5 offers conclusions.

2. The algorithm

With the purpose of showing our algorithm, here is the general statement of the concept of projection operator $P_C(x)$, which represents a mapping from R^n to C a nonempty closed convex set:

$$P_C(x) = \arg\min\{\| z - x \| \, | z \in C\}.$$

$\|\cdot\|$ represents Euclidean norm, which has a character, ie, for any $x \in R^n, z \in C$,

$$\|P_C(x) - z\|^2 \le \|x - z\|^2 - \|x - P_C(x)\|^2. \tag{2.1}$$

The following are the detailed steps of the algorithm.

Algorithm 1 (*ITTPRP*).

Step 0. Input $x_0 = x_{-1} \in R^n$, $\mu, s, \sigma, > 0, 0 < \rho, \varepsilon < 1$ and $0 \le \tau < 1$, Let $m := 0$.

Step 1. If $\|\Omega(x_m)\| \le \varepsilon$, then terminate. Else select an inertial extrapolation steplength

$$\tau_m = \begin{cases} \min\left\{\tau, \frac{1}{k^2\|\Delta x_m\|^2}\right\}, & \text{if } \Delta x_m \neq 0, \\ \tau, & \text{otherwise}, \end{cases} \tag{2.2}$$

and compute the inertial step

$$\upsilon_m = x_m + \tau_m(\Delta x_m),$$

where $\Delta x_m = x_m - x_{m-1}$.

Step 2. If $\|\Omega(\upsilon_m)\| \le \varepsilon$, then terminate. Else find the search direction d_m by

$$d_m = \begin{cases} -\Omega(\upsilon_m) + \frac{\Omega(\upsilon_m)^T y_m d_{m-1} - \Omega(\upsilon_m)^T d_{m-1} y_m}{max\{\mu\|d_{m-1}\|\|y_m\|, \|\Omega(\upsilon_{m-1})\|^2\}}, & \text{if } m \ge 1, \\ -\Omega(\upsilon_m), & \text{if } m = 0, \end{cases}$$

where $y_m = \Omega(\upsilon_m) - \Omega(\upsilon_{m-1})$.

Step 3. Find $t_m = \upsilon_m + \alpha_m d_m$, the steplength $\alpha_m := \max\{s\rho^i : i = 0, 1, 2, \ldots\}$ such that

$$-\Omega(\upsilon_m + \alpha_m d_m)^T d_m \ge \sigma\alpha_m \left\|\Omega(\upsilon_m + \alpha_m d_m)\right\| \left\|d_m\right\|^2. \tag{2.3}$$

Step 4. If $\|\Omega(t_m)\| \le \varepsilon$, terminate, and let $\upsilon_{m+1} = t_m$. Else, calculate the next iterate by

$$x_{m+1} = P_c[\upsilon_m - \lambda_m \Omega(t_m)],$$

where

$$\lambda_m = \frac{\Omega(t_m)^T(\upsilon_m - t_m)}{\|\Omega(t_m)\|^2}.$$

Step 5. Let $m := m + 1$. Back to step 1.

Remark 2.1. For all $m \ge 0$, it can be observed from Eq. (2.2) that $\tau_m\|\Delta x_m\|^2 \le \frac{1}{m^2}$. This implies that

$$\sum_{m=1}^{\infty} \tau_m\|\Delta x_m\|^2 < \infty.$$

Lemma 2.1. *If $\{d_m\}$ and $\{\upsilon_m\}$ are calculated by Algorithm ITTPRP, then d_m satisfies the characteristic of sufficient descent :*

$$\Omega(\upsilon_m)^T d_m = -\|\Omega(\upsilon_m)\|^2 \tag{2.4}$$

and the trust region characteristic:

$$\|d_m\| \le \left(1 + \frac{2}{\mu}\right)\|\Omega(\upsilon_m)\|. \tag{2.5}$$

Proof. By the definition of d_m in Algorithm 1, it is easy to conclude that $\Omega(\upsilon_m)^T d_m = -\|\Omega(\upsilon_m)\|^2$ for all $m \ge 0$. If $m = 0$ or $y_m = 0$, we have $\|d_m\| = \|\Omega(\upsilon_m)\|$. For $k \ge 1$ and $y_m \neq 0$, we can deduce that

$$\begin{aligned} \|d_m\| &\le \left\|\Omega(\upsilon_m)\right\| + \frac{2\|\Omega(\upsilon_m)\|\|y_m\|\|d_{m-1}\|}{max\{\mu\|d_{m-1}\|\|y_m\|, \|\Omega(\upsilon_{m-1})\|^2\}} \\ &\le \left\|\Omega(\upsilon_m)\right\| + \frac{2\|\Omega(\upsilon_m)\|\|y_m\|\|d_{m-1}\|}{\mu\|d_{m-1}\|\|y_m\|} \\ &= (1 + \frac{2}{\mu})\|\Omega(\upsilon_m)\|. \end{aligned} \tag{2.6}$$

The proof is concluded.

3. Global convergence

This section will provide a proof of convergence for the ITTPRP method. Some necessary hypotheses and lemmas are as follows.

Hypothesis A. (i) The solution set S contains at least one valid solution, indicating that the solution set S is non-empty.

(ii) The mapping Ω is Lipschitz continuous, which means there is a positive number M, for any $x, y \in R^n$,

$$\|\Omega(x) - \Omega(y)\| \le M\|x - y\|.$$

Lemma 3.1. *Assume Hypothesis A is always valid, sequences $\{\upsilon_m\}$ and $\{d_m\}$ are formed by the ITTPRP algorithm, then for all $m \ge 0$, there is a nonnegative i_m satisfying inequality (2.3).*

Proof. By using reduction to absurdity, we can obtain the following result: Suppose there exists an integer m_0 greater than 0, which makes all nonnegative integers i fail to satisfy (2.3). Therefore, for all $i \geq 0$, the subsequent inequality is always valid:

$$-\Omega\left(v_{m_0}+s\rho^i d_{m_0}\right)^T d_{m_0} < \sigma s\rho^i \left|\Omega\left(v_{m_0}+s\rho^i d_{m_0}\right)\right| \left|d_{m_0}\right|^2.$$

Consider Ω is continuous and $\rho \in (0,1)$, as $i \to \infty$, it satisfies that $\Omega(v_{m_0})^T d_{m_0} \geq 0$ which contradicts with (2.4). Thus the proof is concluded.

Lemma 3.2 (*Auslender et al., 1999*). *Suppose $\{x_m\}$ and $\{t_m\}$ be nonnegative number sequences, then they satisfy the subsequent inequality:*

$$x_{m+1} \leq x_m + t_m.$$

where $\sum_{m=1}^{\infty} t_m < \infty$, then $\lim_{m\to\infty} x_m$ exists.

Lemma 3.3. *Let hypothesis A hold, and sequences $\{x_m\}$, $\{v_m\}$ and $\{t_m\}$ are successively outputted by Algorithm 1. Assume that $\bar{x}$ represents a solution to problem (1.1) with $\Omega(\bar{x}) = 0$, which satisfies*

$$\|x_{m+1}-\bar{x}\|^2 \leq \|v_m-\bar{x}\|^2 - \sigma^2\|v_m-t_m\|^4.$$

Moreover, the sequence $\{x_m\}$ is bounded and

$$\sum_{m=1}^{\infty} \|v_m-t_m\|^4 < \infty.$$

Proof. Through the monotonicity of the mapping Ω, we can infer

$$\begin{aligned}
\Omega(t_m)^T(v_m-\bar{x}) &= \Omega(t_m)^T(v_m-t_m) + \Omega(t_m)^T(t_m-\bar{x}) \\
&\geq \Omega(t_m)^T(v_m-t_m) + \Omega(\bar{x})^T(t_m-\bar{x}) \\
&= \Omega(t_m)^T(v_m-t_m) \qquad (3.1)\\
&\geq \sigma\|\Omega(t_m)\|\|v_m-t_m\|^2. \qquad (3.2)
\end{aligned}$$

By (2.1), (3.1), and (3.2), it establishes that, for any $\bar{x} \in S$,

$$\begin{aligned}
\|x_{m+1}-\bar{x}\|^2 &= \left\|P_C\left(v_m-\lambda_m\Omega(t_m)\right)-\bar{x}\right\|^2 \\
&\leq \left\|\left(v_m-\lambda_m\Omega(t_m)\right)-\bar{x}\right\|^2 \\
&\quad - \left\|\left(v_m-\lambda_m\Omega(t_m)\right)-P_C\left(v_m-\lambda_m\Omega(t_m)\right)\right\|^2 \\
&\leq \|v_m-\lambda_m\Omega(t_m)-\bar{x}\|^2 \\
&\leq \|v_m-\bar{x}\|^2 - 2\lambda_m\Omega(t_m)^T(v_m-\bar{x}) + \lambda_m^2\|\Omega(t_m)\|^2 \\
&\leq \|v_m-\bar{x}\|^2 - 2\lambda_m\Omega(t_m)^T(v_m-t_m) + \lambda_m^2\|\Omega(t_m)\|^2 \\
&\leq \|v_m-\bar{x}\|^2 - \frac{[\Omega(t_m)^T(v_m-t_m)]^2}{\|\Omega(t_m)\|^2} \\
&\leq \|v_m-\bar{x}\|^2 - \sigma^2\|v_m-t_m\|^4. \qquad (3.3)
\end{aligned}$$

From inequality (3.3), we can deduce that

$$\begin{aligned}
\|x_{m+1}-\bar{x}\| &\leq \|v_m-\bar{x}\| \\
&= \|x_m+\tau_m\Delta x_m-\bar{x}\| \\
&\leq \|x_m-\bar{x}\| + \tau_m\|\Delta x_m\|.
\end{aligned}$$

According to Remark 2.1 and Lemma 3.2, we can conclude that the sequence $\{\|x_m-\bar{x}\|\}$ is bounded. Consequently, for all m, there is a positive number M_0 satisfying

$$\|x_m-\bar{x}\| \leq M_0. \qquad (3.4)$$

Thus, we can infer that $\|\Delta x_m\| \leq 2M_0$. Building upon the aforementioned conclusions, we can derive that

$$\begin{aligned}
\|v_m-\bar{x}\|^2 &= \|x_m+\tau_m\Delta x_m-\bar{x}\|^2 \\
&\leq \|x_m-\bar{x}\|^2 + 2\tau_m\Delta x_m^T(x_m+\tau_m\Delta x_m-\bar{x}) \\
&\leq \|x_m-\bar{x}\|^2 + 2\tau_m\|\Delta x_m\|(\|x_m-\bar{x}\| + \tau_m\|\Delta x_m\|) \\
&\leq \|x_m-\bar{x}\|^2 + 2M_0\tau_m\|\Delta x_m\| + 4M_0\tau_m\|\Delta x_m\| \\
&= \|x_m-\bar{x}\|^2 + 6M_0\tau_m\|\Delta x_m\|. \qquad (3.5)
\end{aligned}$$

By (3.3) and (3.5), We obtain

$$\|x_{m+1}-\bar{x}\|^2 \leq \|x_m-\bar{x}\|^2 + 6M_0\tau_m\|\Delta x_m\| - \sigma^2\|v_m-t_m\|^4.$$

Thus, we have

$$\sigma^2\|v_m-t_m\|^4 \leq \|x_m-\bar{x}\|^2 + 6M_0\tau_m\|\Delta x_m\| - \|x_{m+1}-\bar{x}\|^2. \qquad (3.6)$$

Adding (3.6) for $m = 1, 2, 3 \ldots$, we have

$$\sigma^2\sum_{k=1}^{\infty}\|v_m-t_m\|^4 \leq \sum_{m=1}^{\infty}(\|x_m-\bar{x}\|^2 + 6M_0\tau_m\|\Delta x_m\| - \|x_{m+1}-\bar{x}\|^2).$$

But $\sum_{m=1}^{\infty}(\|x_m-\bar{x}\|^2 - \|x_{m+1}-\bar{x}\|^2)$ is finite, which is due to the sequence $\{\|x_{m+1}-\bar{x}\|\}$ is convergent and $\sum_{m=1}^{\infty}\tau_m\|\Delta x_m\| < \infty$. It implies that

$$\sigma^2\sum_{m=1}^{\infty}\|v_m-t_m\|^4 \leq \sum_{m=1}^{\infty}(\|x_m-\bar{x}\|^2 - \|x_{m+1}-\bar{x}\|^2 + 6M_0\tau_m\|\Delta x_m\|) < \infty.$$

Therefore,

$$\lim_{m\to\infty}\|v_m-t_m\| = 0. \qquad (3.7)$$

Finally, this proof is concluded.

Remark 3.1. If Hypothesis A is always valid, we can deduce the following conclusions from Lemma 3.3.

(i) The $\|\Omega(x)\|$ is bounded.
(ii) $\lim_{m\to\infty}\|x_m-v_m\| = \lim_{m\to\infty}\|v_m-t_m\| = \lim_{m\to\infty}\alpha_m\|d_m\| = 0$.
(iii) The sequences $\{x_m\}$, $\{v_m\}$, $\{t_m\}$ and $\{d_m\}$ are all bounded.

Proof. (i) From Hypothesis A(ii) and (3.4), we have

$$\|\Omega(x)\| = \|\Omega(x)-\Omega(\bar{x})\| \leq M\|x-\bar{x}\| \leq MM_0.$$

(ii) By the concept of $\{t_m\}$ and (3.7), having $\lim_{m\to\infty}\alpha_m\|d_m\| = 0$, What is more, from Remark 2.1, considering that $\sum_{m=1}^{\infty}\tau_m\|\Delta x_m\| < \infty$, we can infer that

$$\lim_{m\to\infty}\|x_m-v_m\| = \lim_{m\to\infty}\|x_m-\left(x_m+\tau_m\Delta x_m\right)\| = \lim_{m\to\infty}\tau_m\|\Delta x_m\| = 0.$$

Thus,

$$\lim_{m\to\infty}\|x_m-v_m\| = \lim_{m\to\infty}\|v_m-t_m\| = \lim_{m\to\infty}\alpha_m\|d_m\| = 0. \qquad (3.8)$$

(iii) The sequence $\{x_m\}$ is bounded, which can be seen from Lemma 3.3. Thus, we can infer that both $\{v_m\}$ and $\{t_m\}$ are also bounded from (3.8). Based on this facts and using Lemma 2.1 and the continuity of Ω, we can conclude that $\{d_m\}$ is bounded. Then the proof is finished.

Theorem 3.1. *If Hypothesis A is always valid. Let $\{x_m\}$, $\{v_m\}$ and $\{t_m\}$ are generated by ITTPRP, and $\bar{x}$ belongs to S. Then, the convergence of $\{x_m\}$, $\{v_m\}$ and $\{t_m\}$ to the same solution of problem (1.1) is ensured.*

Proof. The proof will be divided into two parts.

Part I. We should exhibit that $\liminf_{m\to\infty}\|\Omega(v_m)\| = 0$. We will demonstrate this by reduction to absurdity, starting with the assumption that

$$\lim_{m\to\infty}\inf\|\Omega(v_m)\| \neq 0.$$

Hence, there is a constant $\epsilon > 0$ satisfying

$$\|\Omega(v_m)\| \geq \epsilon, \ \forall\ m \geq 0. \qquad (3.9)$$

Based on the bondedness of $\{v_m\}$ and $\{d_m\}$, we can infer

$$\lim_{i\to\infty} v_{m_i} = \bar{v} \text{ and } \lim_{i\to\infty} d_{m_i} = \bar{d}. \qquad (3.10)$$

By setting $m := m_i$ in (2.4), and utilizing (3.9), (3.10) and the continuity of Ω. Finally, taking the limit of (2.4), we can obtain

$$\Omega(\bar{v})^T\bar{d} = -\|\Omega(\bar{v})\|^2 \leq -\epsilon^2 < 0. \qquad (3.11)$$

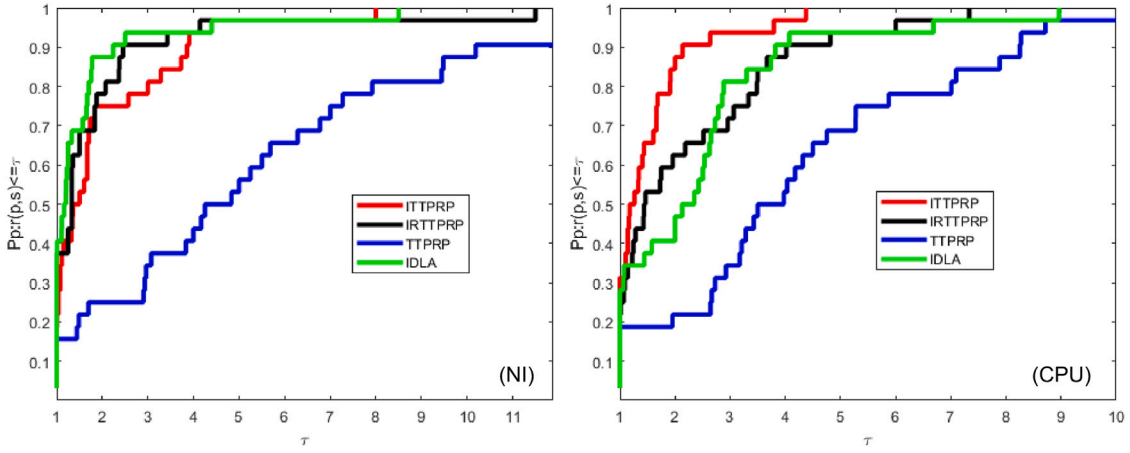

Fig. 1. Performance profiles on NI and CPU.

By the definition of d_m, we then obtain that $\|d_m\| \geq \|\Omega(\upsilon_m)\| \geq \epsilon$, which, combined with Remark 3.1(ii), indicates the limit $\lim_{m\to\infty} \alpha_m = 0$. Finally, from (2.3), it satisfies

$$-\Omega(\upsilon_m + \rho^{-1}\alpha_m d_m)^T d_m < \sigma\rho^{-1}\alpha_m \|\Omega(\upsilon_m + \rho^{-1}\alpha_m d_m)\| \|d_m\|^2. \tag{3.12}$$

Consider all m satisfying sufficiently large characteristics. Similarly, together with (3.12), Remark 3.1(ii), (3.10) and $\lim_{m\to\infty} \alpha_m = 0$, one can ensure $\Omega(\bar{\upsilon})^T \bar{d} \geq 0$, which contradicts with (3.11). Consequently, we deduce that $\liminf_{m\to\infty} \|\Omega(\upsilon_m)\| = 0$.

Part II. We show that $\{x_m\}$, $\{\upsilon_m\}$, and $\{t_m\}$ all converge to the same solution of problem (1.1). Since $\{\upsilon_m\}$ is bounded, Ω is a continuous mapping, and the previous part has already established that $\lim_{m\to\infty} \inf \|\Omega_m\| = 0$. Based on these, we assume

$$\lim_{i\to\infty} \| \Omega(\upsilon_{m_i}) \| = \| \Omega(\bar{\upsilon}) \| = 0,$$

which indicates $\bar{\upsilon} \in S$. Based on the first relation in (3.10) and Remark 3.1(ii), we can obtain $\bar{\upsilon}$ is a convergence point of $\{x_m\}$, implying there is an infinite set $\mathcal{M}$ satisfying $\lim_{m\in\mathcal{M}, m\to\infty} x_m = \bar{\upsilon} \in S$. Setting $\bar{x} := \bar{\upsilon}$ in Remark 3.1(ii), we have

$$\lim_{m\to\infty} \|x_m - \bar{\upsilon}\| = \lim_{m\in K, m\to\infty} \|x_m - \bar{\upsilon}\| = 0.$$

So, $\{x_m\}$ converges to $\bar{\upsilon} \in S$. Based on Remark 3.1(ii), we can infer that both $\{\upsilon_m\}$ and $\{t_m\}$ also converge to $\bar{\upsilon}$. This proof is concluded.

4. Numerical results and discussions

Numerical experiments will be conducted in two modules. The first module involves solving nonlinear equations, while the second module focuses on an image restoration application.

4.1. Nonlinear equations

We conduct tests on nonlinear equations in this module. The problems to be tested and their corresponding initial points can be found in Yuan and Zhang (2015). For experimentation, we utilize the eight problems listed in Table 1, maintaining the same initial points as those in Yuan and Zhang (2015).

To demonstrate the superiority of the ITTPRP algorithm, We compared it to the IDLA algorithm (Sabi'U and Sirisubtawee, 2024), the TTPRP algorithm (Yuan and Zhang, 2015), and the inertial-relaxed TTPRP method which differs from ITTPRP by maintaining $\tau_k \equiv \tau$ and introducing a relaxation factor ρ_k in the projection step. Detailed information regarding the inertial-relaxed technique can be found in Yin et al. (2023). In this article, we refer to the inertial-relaxed TTPRP method as the IRTTPRP method.

The following were used for experimental comparison:

Table 1
Test problems.

NO	Test problem
1	Exponential function
2	Trigonometric function
3	Logarithmic function
4	Broyden tridiagonal function
5	Trigexp function
6	Strictly convex function
7	Extended Freudentein and Roth function
8	Discrete boundary value problem

- Dimensions: 5000, 10,000, 50,000, 100,000.
- Parameters: We select $\sigma = 0.01, \mu = 0.01, s = 1, \rho = 0.1, \tau = 0.1$ and $\epsilon = 10^{-4}$ for ITTPRP. Furthermore, we set the relaxation factor $\rho_k \equiv 1.4882$ for IRTTPRP and other parameters are consistent with ITTPRP. For TTPRP and IDLA, all parameters are cited from Yuan and Zhang (2015) and Sabi'U and Sirisubtawee (2024), respectively.
- Stopping condition: The operations are terminated when any of the subsequent criteria is met: (i) $\|\Omega(x_m)\| \leq 10^{-4}$, (ii) $\|\Omega(\upsilon_m)\| \leq 10^{-4}$, (iii) $\|\Omega(t_m)\| \leq 10^{-4}$, (iv) $NI > 1000$.
- Implementation software: All experiments are operated in MATLAB R2020a on a 64-bit Lenovo laptop with lntel(R) Core(TM) i5-7200U CPU (2.70 GHz), 8.00 GB RAM and Windows 10.

The results from these methods are presented in Tables 2–5, where NO denotes the problem number, DIM indicates the dimension of the variable x, IN represents the number of iterations, CPU signifies the running time in seconds, and GN refers the norm of the objective function. As illustrated in Fig. 1, ITTPRP, IRTTPRP, and IDLA significantly outperform TTPRP for nonlinear equations, suggesting that both inertial and inertial-relaxed techniques can enhance the convergence of the algorithm. Furthermore, the numerical results regarding NI and CPU demonstrate that the ITTPRP method outperforms both the IDLA and IRTTPR methods.

4.2. Image restoration problems

The objective of this part is to restore images that have been compromised by salt-and-pepper noise to their original state. The operating conditions and parameters remain consistent with those outlined in the previous section. The termination condition is $\frac{|\|\Omega(x_{m+1})\| - \|\Omega(x_m)\||}{\|\Omega(x_m)\|} < 10^{-3}$ or $\frac{\|x_{m+1} - x_m\|}{\|x_m\|} < 10^{-3}$. For the experiments, we selected the images Peppers ($384 \times 512 \times 3$), ColoredChips ($391 \times 518 \times 3$) and ColorChecker ($1024 \times 1541 \times 3$) as subjects. To facilitate a comparison with ITTPRP, we also implemented IDLA, IRTTPRP, and TTPRP in our experiments. In this study, we employed the Peak Signal-to-Noise Ratio (PSNR) as a

Table 2
The numerical results of ITTPRP.

NO	Dim	ITTPRP			NO	Dim	ITTPRP		
		NI	CPU	GN			NI	CPU	GN
1	5000	12	0.453125	9.867163e−05	5	5000	27	0.28125	8.497070e−05
	10 000	26	0.734375	8.790935e−05		10 000	31	0.515625	8.141910e−05
	50 000	16	1.640625	9.210669e−05		50 000	27	1.625	8.768074e−05
	100 000	29	4.5625	8.383628e−05		100 000	27	2.640625	7.807696e−05
2	5000	11	0.0625	3.770076e−05	6	5000	41	0.21875	9.759364e−05
	10 000	10	0.125	9.709109e−05		10 000	43	0.734375	8.647722e−05
	50 000	10	0.328125	3.639045e−05		50 000	46	1.359375	9.793179e−05
	100 000	10	0.703125	6.912180e−05		100 000	48	3.03125	8.597722e−05
3	5000	46	0.359375	8.099398e−05	7	5000	96	0.96875	7.257720e−05
	10 000	47	0.578125	9.131047e−05		10 000	99	1.875	7.786170e−04
	50 000	54	2.0625	8.278900e−05		50 000	99	5.25	4.462174e−04
	100 000	57	4.34375	7.885919e−05		100 000	99	9.109375	2.193503e−02
4	5000	28	0.125	8.043680e−05	8	5000	4	0.03125	6.854517e−05
	10 000	28	0.375	9.621304e−05		10 000	4	0.078125	3.561221e−05
	50 000	30	0.9375	9.573799e−05		50 000	4	0.25	9.843457e−06
	100 000	31	1.796875	8.726494e−05		100 000	4	0.5	6.258972e−06

Table 3
The numerical results of IRTTPRP.

NO	Dim	IRTTPRP			NO	Dim	IRTTPRP		
		NI	CPU	GN			NI	CPU	GN
1	5000	19	0.828125	7.836595e−05	5	5000	25	0.34375	6.204524e−05
	10 000	20	0.703125	8.971482e−05		10 000	27	0.4375	6.786293e−05
	50 000	23	2.75	6.002047e−05		50 000	25	1.421875	9.841160e−05
	100 000	24	3.6875	9.233313e−05		100 000	29	3.671875	5.259499e−05
2	5000	11	0.171875	9.408117e−05	6	5000	26	0.234375	8.169599e−05
	10 000	11	0.15625	6.641194e−05		10 000	27	0.34375	8.119625e−05
	50 000	8	0.296875	8.029260e−05		50 000	29	1.234375	8.995054e−05
	100 000	8	0.640625	4.743628e−05		100 000	30	2.109375	8.960796e−05
3	5000	34	0.65625	9.324219e−05	7	5000	60	0.984375	9.753238e−05
	10 000	35	1.015625	9.390085e−05		10 000	58	1.609375	2.541513e−05
	50 000	28	1.484375	7.782818e−05		50 000	89	6	8.480105e−05
	100 000	43	2.84375	7.892516e−05		100 000	98	11.328125	8.867816e−05
4	5000	27	0.21875	7.681626e−05	8	5000	6	0.1875	9.285473e−05
	10 000	27	0.296875	9.770017e−05		10 000	6	0.15625	5.875351e−05
	50 000	40	3.265625	6.750844e−05		50 000	5	0.546875	6.323570e−05
	100 000	42	7.21875	6.956756e−05		100 000	5	1.140625	4.472713e−05

Table 4
The numerical results of TTPRP.

NO	Dim	TTPRP			NO	Dim	TTPRP		
		NI	CPU	GN			NI	CPU	GN
1	5000	8	0.171875	5.520721e−05	5	5000	198	1.484375	9.447610e−05
	10 000	15	0.546875	9.436249e−05		10 000	183	1.828125	9.199929e−05
	50 000	2	0.375	5.758779e−05		50 000	236	7.5	9.513637e−05
	100 000	7	1.203125	8.972378e−05		100 000	217	13.140625	9.726429e−05
2	5000	30	0.484375	9.362377e−05	6	5000	77	0.578125	9.444245e−05
	10 000	29	0.375	8.383729e−05		10 000	80	0.9375	9.681243e−05
	50 000	25	1.421875	9.255956e−05		50 000	88	3.609375	9.197911e−05
	100 000	23	2.078125	9.365469e−05		100 000	91	6.765625	9.440982e−05
3	5000	49	0.5	9.118515e−05	7	5000	833	6.875	9.922871e−05
	10 000	52	0.671875	9.408785e−05		10 000	857	13.28125	9.916437e−05
	50 000	21	1.03125	8.293763e−05		50 000	907	41.40625	9.868439e−05
	100 000	73	8.5625	9.228799e−05		100 000	929	79.375	9.970836e−05
4	5000	80	0.734375	9.669655e−05	8	5000	22	0.140625	8.867872e−05
	10 000	83	1.28125	8.554486e−05		10 000	21	0.046875	7.910912e−05
	50 000	88	3.78125	8.746539e−05		50 000	17	0.875	9.143833e−05
	100 000	90	7.140625	9.043480e−05		100 000	16	1.4375	8.204131e−05

metric to assess the effectiveness of the image restoration. Generally, a higher PSNR value for the restored image indicates superior performance of the restoration algorithm. The detailed performances are illustrated in Figs. 2–4. It is evident that four algorithms successfully restored the images. Table 6 presents the PSNR values corresponding to the restored images obtained from these three methods. The results show that at noise levels of 20%, 40%, and 60%, the PSNR values for ITTPRP exceed those of IDLA, IRTTPRP, and TTPRP, suggesting that the ITTPRP algorithm outperforms the others.

5. Conclusions

The primary contribution of this article is the proposal of an inertial three-term PRP CG projection method for large-scale nonlinear equations. This method achieves global convergence under appropriate assumptions. The experimental results demonstrate that the incorporation of the extrapolation strategy significantly accelerates the algorithm's iteration. Furthermore, a comparison of various methods for image restoration problems clearly illustrates the superiority and effectiveness

Table 5
The numerical results of IDLA.

NO	Dim	IDLA			NO	Dim	IDLA		
		NI	CPU	GN			NI	CPU	GN
1	5000	20	0.65625	7.992.25e−05	5	5000	25	0.40625	7.366243e−05
	10 000	66	3.65625	9.846248e−05		10 000	33	1.0625	7.053033e−05
	50 000	17	3.359375	NaN		50 000	44	4.6875	6.881303e−05
	100 000	11	4.5	NaN		100 000	7	1.875	NaN
2	5000	6	0.046875	7.682945e−06	6	5000	11	0.625	9.534414e−05
	10 000	6	0.109375	5.511686e−06		10 000	11	0.9375	7.814199e−05
	50 000	6	0.171875	9.212817e−05		50 000	14	3.4375	6.859685e−05
	100 000	6	0.4375	7.765051e−05		100 000	16	8.59375	6.634121e−05
3	5000	41	0.1875	9.624785e−05	7	5000	99	2.0625	3.698474e+01
	10 000	42	0.34375	9.784315e−05		10 000	99	3.78125	3.076731e+01
	50 000	47	1.109375	9.630625e−05		50 000	99	13.921875	2.315295e+02
	100 000	50	2.609375	9.159562e−05		100 000	99	22.8125	4.025442e+02
4	5000	36	0.328125	6.010409e−05	8	5000	5	0.0625	6.044117e−05
	10 000	30	0.46875	9.152611e−05		10 000	5	0.09375	5.190158e−05
	50 000	50	2.375	4.619752e−05		50 000	4	0.265625	7.682776e−05
	100 000	55	5.171875	9.349308e−05		100 000	4	0.453125	6.073980e−05

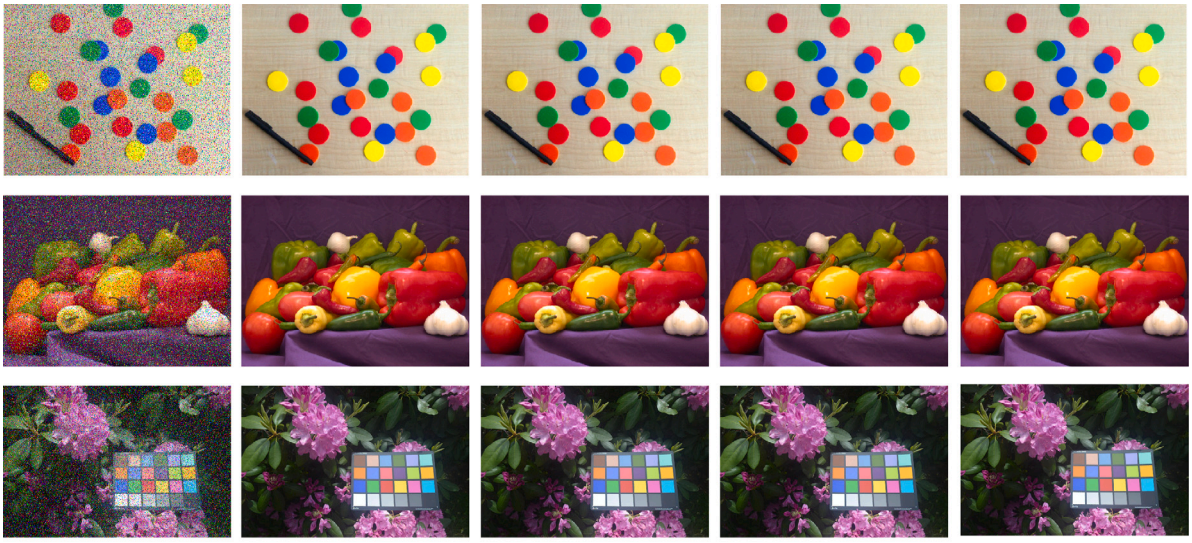

Fig. 2. The restored images of ColoredChips, Peppers and ColorChecker with 20% salt-and-pepper noise by ITTPRP method, IRTTPRP method, TTPRP method and IDLA method are displayed respectively from left to right.

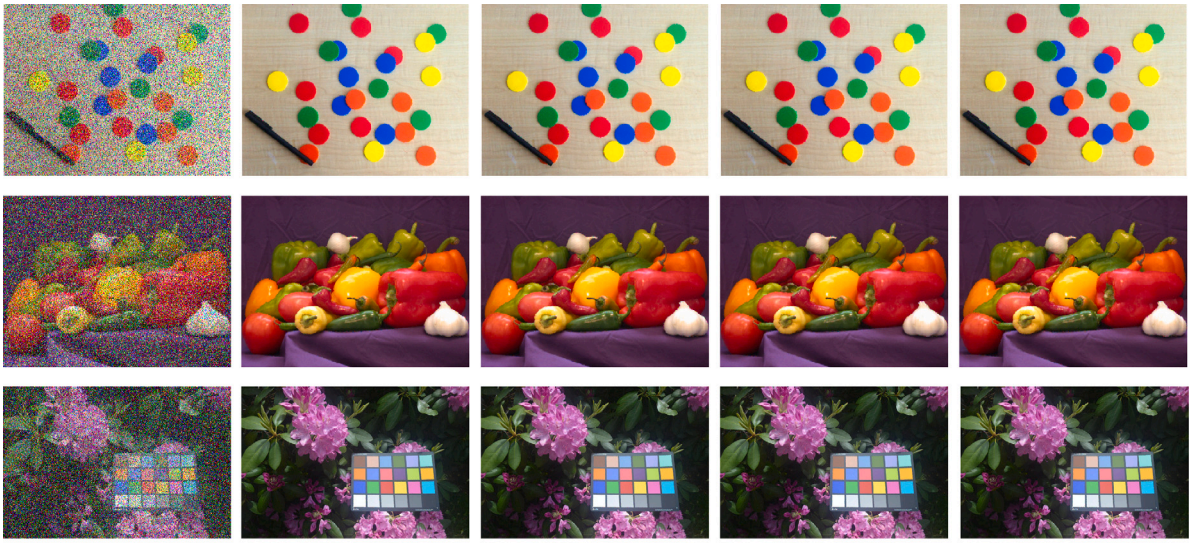

Fig. 3. The restored images of ColoredChips, Peppers and ColorChecker with 40% salt-and-pepper noise by ITTPRP method, IRTTPRP method, TTPRP method and IDLA method are displayed respectively from left to right.

Fig. 4. The restored images of ColoredChips, Peppers and ColorChecker with 60% salt-and-pepper noise by ITTPRP method, IRTTPRP method, TTPRP method and IDLA method are displayed respectively from left to right.

Table 6
Three algorithms restore image PSNR value.

20% noise	Peppers	ColoredChips	ColarChecker
ITTPRP	39.25	39.60	40.71
IRTTPRP	39.36	39.52	40.62
TTPRP	39.18	39.40	40.60
IDLA	39.11	39.51	41.09
40% noise	Peppers	ColoredChips	ColarChecker
ITTPRP	34.72	34.79	36.27
IRTTPRP	34.60	34.80	36.29
TTPRP	34.52	34.56	36.22
IDLA	34.19	34.39	35.84
60% noise	Peppers	ColoredChips	ColarChecker
ITTPRP	31.24	31.13	32.81
IRTTPRP	31.22	31.12	32.75
TTPRP	30.87	30.35	32.72
IDLA	30.97	30.48	32.04

of the ITTPRP algorithm. This image restoration technique has the potential to enhance video surveillance, medical image processing, and various other practical applications, paving the way for further research and technological development.

CRediT authorship contribution statement

Gonglin Yuan: Writing – review & editing, Supervision, Funding acquisition. **Chunzhao Liang:** Writing – original draft, Visualization, Validation, Software, Resources, Methodology, Investigation, Formal analysis, Data curation, Conceptualization. **Yong Li:** Writing – review & editing, Supervision.

Declaration of competing interest

The authors declare that they have no known competing financial interests or personal relationships that could have appeared to influence the work reported in this paper.

Acknowledgments

This work is supported by Guangxi Science and Technology base and Talent Project, PR China (Grant No. AD22080047), the major talent project of Guangxi (GXR-6BG242404), the special foundation for Guangxi Ba Gui Scholars, the Innovation Project of Guangxi Graduate Education, PR China (Grant No. YCBZ2024001), and the Guangxi Natural Science Foundation, PR China (Grant No. 2024GXNSFAA999149). Thanks to the editor and reviewers for their valuable comments, which greatly improved the quality of the paper.

References

Abubakar, J., Kumam, P., Hassan Ibrahim, A., Padcharoen, A., 2020a. Relaxed inertial Tseng's type method for solving the inclusion problem with application to image restoration. Mathematics 8, 818.
Abubakar, J., Kumam, P., Rehman, H.U., Hassan Ibrahim, A., 2020b. Inertial iterative schemes with variable step sizes for variational inequality problem involving pseudomonotone operator. Mathematics 8, 609.
Abubakar, A.B., Sabi'U, J., Kumam, P., Shah, A., 2021. Solving nonlinear monotone operator equations via modified sr1 update. J. Appl. Math. Comput. 1–31.
Abubakar, J., Sombut, K., Ibrahim, A.H., 2019. An accelerated subgradient extragradient algorithm for strongly pseudomonotone variational inequality problems. Thai J. Math. 18, 166–187.
Alvarez, F., 2004. Weak convergence of a relaxed and inertial hybrid projection-proximal point algorithm for maximal monotone operators in Hilbert space. SIAM J. Optim. 14, 773–782.
Alvarez, F., Attouch, H., 2001. An inertial proximal method for maximal monotone operators via discretization of a nonlinear oscillator with damping. Set-Valued Anal. 9, 3–11.
Auslender, A., Teboulle, M., BenTiba, S., 1999. A logarithmic-quadratic proximal method for variational inequalities. In: Computational Optimization: A Tribute to Olvi Mangasarian. vol. I, pp. 31–40.
Chen, C., Chan, R.H., Ma, S., Yang, J., 2015. Inertial proximal admm for linearly constrained separable convex optimization. SIAM J. Imaging Sci. 8, 2239–2267.
Chen, Z., Cheng, W., Li, X., 2014. A global convergent quasi-Newton method for systems of monotone equations. J. Appl. Math. Comput. 44, 455–465.
Chen, P., Huang, J., Zhang, X., 2013. A primal–dual fixed point algorithm for convex separable minimization with applications to image restoration. Inverse Problems 29, 025011.
Gregory, J., Zeman, M., Badiey, M., 1985. A finite element approximation for the initial-value problem for nonlinear second-order differential equations. J. Math. Anal. Appl. 111, 90–104.
Ibrahim, A.H., Kumam, P., Abubakar, A.B., Abubakar, J., 2021. A method with inertial extrapolation step for convex constrained monotone equations. J. Inequal. Appl. 2021, 189.
Iiduka, H., 2012. Iterative algorithm for triple-hierarchical constrained nonconvex optimization problem and its application to network bandwidth allocation. SIAM J. Optim. 22, 862–878.
Jian, J., Yin, J., Tang, C., Han, D., 2022. A family of inertial derivative-free projection methods for constrained nonlinear pseudo-monotone equations with applications. Comput. Appl. Math. 41, 309.
Jolaoso, L., Alakoya, T., Taiwo, A., Mewomo, O., 2021. Inertial extragradient method via viscosity approximation approach for solving equilibrium problem in Hilbert space. Optimization 70, 387–412.

Koorapetse, M., Kaelo, P., Lekoko, S., Diphofu, T., 2021. A derivative-free rmil conjugate gradient projection method for convex constrained nonlinear monotone equations with applications in compressive sensing. Appl. Numer. Math. 165, 431–441.

Liu, J., Feng, Y., 2019. A derivative-free iterative method for nonlinear monotone equations with convex constraints. Numer. Algorithms 82, 245–262.

Ma, G., Jin, J., Jian, J., Yin, J., Han, D., 2023. A modified inertial three-term conjugate gradient projection method for constrained nonlinear equations with applications in compressed sensing. Numer. Algorithms 92, 1621–1653.

Meintjes, K., Morgan, A.P., 1987. A methodology for solving chemical equilibrium systems. Appl. Math. Comput. 22, 333–361.

Pock, T., Sabach, S., 2016. Inertial proximal alternating linearized minimization (ipalm) for nonconvex and nonsmooth problems. SIAM J. Imaging Sci. 9, 1756–1787.

Polyak, B.T., 1964. Some methods of speeding up the convergence of iteration methods. USSR Comput. Math. Math. Phys. 4, 1–17.

Qi, L., Tong, X., Li, D., 2004. Active-set projected trust-region algorithm for box-constrained nonsmooth equations. J. Optim. Theory Appl. 120, 601–625.

Sabi'u, J., Balili, A., Emadifar, H., 2024. An efficient Dai-Yuan projection-based method with application in signal recovery. PLoS One 19, 1–26.

Sabi'u, J., Shah, A., Waziri, M.Y., 2020. Two optimal Hager–Zhang conjugate gradient methods for solving monotone nonlinear equations. Appl. Numer. Math. 153, 217–233.

Sabi'U, J., Shah, A., Waziri, M.Y., Dauda, M.K., 2020. A new hybrid approach for solving large-scale monotone nonlinear equations. J. Math. Fundam. Sci. 52, 17–26.

Sabi'U, J., Sirisubtawee, S., 2024. An inertial Dai-Liao conjugate method for convex constrained monotone equations that avoids the direction of maximum magnification. J. Appl. Math. Comput. 70, 4319–4351.

Solodov, M.V., Svaiter, B.F., 1999. A globally convergent inexact Newton method for systems of monotone equations. In: Reformulation: Nonsmooth, piecewise smooth, semismooth and smoothing methods. pp. 355–369.

Ulbrich, M., 2001. Nonmonotone trust-region methods for bound-constrained semismooth equations with applications to nonlinear mixed complementarity problems. SIAM J. Optim. 11, 889–917.

Xiao, X., Li, Y., Wen, Z., Zhang, L., 2018. A regularized semi-smooth newton method with projection steps for composite convex programs. J. Sci. Comput. 76, 364–389.

Xiao, Y., Wang, Q., Hu, Q., 2011. Non-smooth equations based method for 1-norm problems with applications to compressed sensing. Nonlinear Anal. TMA 74, 3570–3577.

Yin, J., Jian, J., Jiang, X., 2021a. A generalized hybrid cgpm-based algorithm for solving large-scale convex constrained equations with applications to image restoration. J. Comput. Appl. Math. 391, 113423.

Yin, J., Jian, J., Jiang, X., Liu, M., Wang, L., 2021b. A hybrid three-term conjugate gradient projection method for constrained nonlinear monotone equations with applications. Numer. Algorithms 88, 389–418.

Yin, J., Jian, J., Jiang, X., Wu, X., 2023. A family of inertial-relaxed dfpm-based algorithms for solving large-scale monotone nonlinear equations with application to sparse signal restoration. J. Comput. Appl. Math. 419, 114674.

Yuan, G., Zhang, M., 2015. A three-terms Polak–Ribière–Polyak conjugate gradient algorithm for large-scale nonlinear equations. J. Comput. Appl. Math. 286, 186–195.

Zhou, W., Li, D., 2007. Limited memory bfgs method for nonlinear monotone equations. J. Comput. Math. 89–96.

Zhou, W., Li, D., 2008. A globally convergent bfgs method for nonlinear monotone equations without any merit functions. Math. Comp. 77, 2231–2240.

Zhou, G., Toh, K., 2005. Superlinear convergence of a newton-type algorithm for monotone equations. J. Optim. Theory Appl. 125, 205–221.